Siderophore-based microbial adaptations to iron scarcity across the eastern Pacific Ocean

Rene M. Boiteau[a,b], Daniel R. Mende[c], Nicholas J. Hawco[a,b], Matthew R. McIlvin[a], Jessica N. Fitzsimmons[b,d], Mak A. Saito[a], Peter N. Sedwick[e], Edward F. DeLong[c], and Daniel J. Repeta[a,1]

[a]Department of Marine Chemistry and Geochemistry, Woods Hole Oceanographic Institution, Woods Hole, MA 02543; [b]Department of Earth, Atmospheric, and Planetary Sciences, Massachusetts Institute of Technology, Cambridge, MA 02139; [c]Center for Microbial Oceanography Research and Education, University of Hawaii at Manoa, Honolulu, HI 96822; [d]Department of Oceanography, Texas A&M University, College Station, TX 77843; and [e]Department of Ocean, Earth and Atmospheric Sciences, Old Dominion University, Norfolk, VA 23529

Edited by W. Ford Doolittle, Dalhousie University, Halifax, NS, Canada, and approved November 7, 2016 (received for review June 1, 2016)

Nearly all iron dissolved in the ocean is complexed by strong organic ligands of unknown composition. The effect of ligand composition on microbial iron acquisition is poorly understood, but amendment experiments using model ligands show they can facilitate or impede iron uptake depending on their identity. Here we show that siderophores, organic compounds synthesized by microbes to facilitate iron uptake, are a dynamic component of the marine ligand pool in the eastern tropical Pacific Ocean. Siderophore concentrations in iron-deficient waters averaged 9 pM, up to fivefold higher than in iron-rich coastal and nutrient-depleted oligotrophic waters, and were dominated by amphibactins, amphiphilic siderophores with cell membrane affinity. Phylogenetic analysis of amphibactin biosynthetic genes suggests that the ability to produce amphibactins has transferred horizontally across multiple Gammaproteobacteria, potentially driven by pressures to compete for iron. In coastal and oligotrophic regions of the eastern Pacific Ocean, amphibactins were replaced with lower concentrations (1–2 pM) of hydrophilic ferrioxamine siderophores. Our results suggest that organic ligand composition changes across the surface ocean in response to environmental pressures. Hydrophilic siderophores are predominantly found across regions of the ocean where iron is not expected to be the limiting nutrient for the microbial community at large. However, in regions with intense competition for iron, some microbes optimize iron acquisition by producing siderophores that minimize diffusive losses to the environment. These siderophores affect iron bioavailability and thus may be an important component of the marine iron cycle.

iron ligands | siderophores | marine microbes | high nutrient low chlorophyll | GEOTRACES

Marine photosynthesis, respiration, and nitrogen fixation all depend on enzymes that require iron (1), which is supplied to the ocean by atmospheric dust deposition, release from sediments, and deep sea hydrothermal activity (2, 3). High biological demand in the sunlit portion of the marine water column, particularly in open ocean regions remote from continental inputs, can decrease dissolved iron (dFe) concentrations to <0.2 nM (2). These regions are often characterized by high-nutrient, low-chlorophyll (HNLC) conditions because iron scarcity limits phytoplankton growth and prevents complete macronutrient utilization (4, 5). Up to 99% of dFe in seawater is complexed by naturally occurring organic ligands (6). Ligands keep otherwise insoluble Fe(III) in solution but may also change its bioavailability. For example, addition of strong iron-binding ligands to seawater has been shown to inhibit iron uptake by plankton, despite high total dFe concentrations (7). Similarly, iron binding polysaccharides have been shown to increase iron uptake rates of natural populations of phytoplankton relative to bacterioplankton (8). The bioavailability of naturally occurring dFe–organic ligand complexes, rather than the total concentration of dFe itself, may therefore be the most important factor regulating microbial production in iron-deficient regions of the ocean.

The sources and composition of natural dFe ligands are largely unknown, but their concentrations and binding strengths have been well constrained by electrochemical measurements. Weak ligands with conditional stability constants ($K^{cond}_{Fe'}$) of 10^{11}–10^{12} exist throughout the water column and may include compounds such as humic substances and acidic polysaccharides (6). In addition, a stronger ligand class with $K^{cond}_{Fe'} > 10^{12}$ is generally present in the surface ocean. The conditional stability constants of these strong ligands are comparable to siderophores (6), chelating agents that are secreted by microbes to bind iron in a form that can be assimilated via active membrane transporters. Metagenomic surveys hint that homologs to known siderophore uptake genes are common in iron-deficient ocean regions, even though siderophore biosynthesis genes themselves have not been found there (9, 10). Siderophore production may be an important strategy to capture iron from the marine environment while preventing uptake by competitors that lack appropriate acquisition pathways.

The prevalence of siderophore-mediated iron acquisition in HNLC regions remains a matter of debate. Diffusive loss of siderophores makes them a potentially costly means of iron acquisition (11), and few siderophores have been directly identified in the marine environment (6, 12). Alternative uptake mechanisms that rely on the reduction of ligand-bound Fe(III) to bioavailable Fe(II) (13) may be energetically favored in iron-poor HNLC regions, although their effectiveness also depends on the

Significance

Iron limits marine production across one third of the surface ocean. The chemical form of iron in these regions is unknown, but it is well established that molecular speciation affects microbial competition for iron uptake. Here we show that the abundance and identity of siderophores, strong iron-binding compounds secreted by microbes to enhance iron uptake, changes across iron-replete and iron-deficient regions of the South Pacific Ocean. In low-iron regions, amphiphilic siderophores are particularly abundant, suggesting a microbial strategy designed to minimize diffusive loss of metabolically expensive compounds while facilitating iron acquisition. Phylogenetic analysis further suggests that the ability to produce amphiphilic siderophores has been transferred across multiple bacterial lineages, suggesting a possible mechanism of adaptation.

Author contributions: R.M.B. and D.J.R. designed research; R.M.B., D.R.M., N.J.H., M.R.M., and P.N.S. performed research; R.M.B., M.R.M., and J.N.F. contributed new reagents/analytic tools; R.M.B., D.R.M., J.N.F., M.A.S., P.N.S., E.F.D., and D.J.R. analyzed data; and R.M.B., D.R.M., N.J.H., M.A.S., P.N.S., E.F.D., and D.J.R. wrote the paper.

The authors declare no conflict of interest.

This article is a PNAS Direct Submission.

Freely available online through the PNAS open access option.

Data deposition: Orbitrap mass spectrometry data are available as a MassIVE (massive.ucsd.edu) dataset (accession no. MSV000080173).

[1]To whom correspondence should be addressed. Email: drepeta@whoi.edu.

This article contains supporting information online at www.pnas.org/lookup/suppl/doi:10.1073/pnas.1608594113/-/DCSupplemental.

speciation and lability of exogenous iron ligand complexes. Ultimately, productivity in iron-deficient regions of the ocean relies on the viability of microbial iron acquisition strategies and thus depends on the composition of the iron ligand pool.

The eastern tropical and subtropical South Pacific Ocean is one of the most productive regions in the world's oceans, with high nutrient concentrations supplied by intense wind-driven upwelling along the coast of South America (Fig. 1, coastal) (5). As surface waters circulate westward, macronutrients and iron are consumed by fast growing microplankton. Dissolved iron is depleted more rapidly than macronutrients (4, 5), shifting the microbial community to smaller nanoplankton that can use the limited iron stocks more efficiently (Fig. 1, HNLC). Eventually, nitrate becomes depleted as well, and nanoplankton are replaced by cyanobacteria and picoeukaryotes that effectively compete for the lower concentrations of macronutrients (Fig. 1, oligotrophic). These natural gradients of iron, nutrients, and microbial communities provided an ideal setting to investigate microbial adaptations to iron availability, as reflected in the distribution, variability, and concentration of different iron ligands, which is the focus of this study. To characterize iron ligand composition at the molecular level, we developed an approach that combines trace metal clean reverse phase liquid chromatography-inductively coupled plasma mass spectrometry (LC-ICPMS) and electrospray ionization mass spectrometry (LC-ESIMS) with metal isotope pattern detection algorithms to detect, identify, and quantify trace metal ligand complexes. Using this approach, we compared the chemical composition of iron ligands across iron-replete and iron-deficient regions of the eastern tropical South Pacific Ocean.

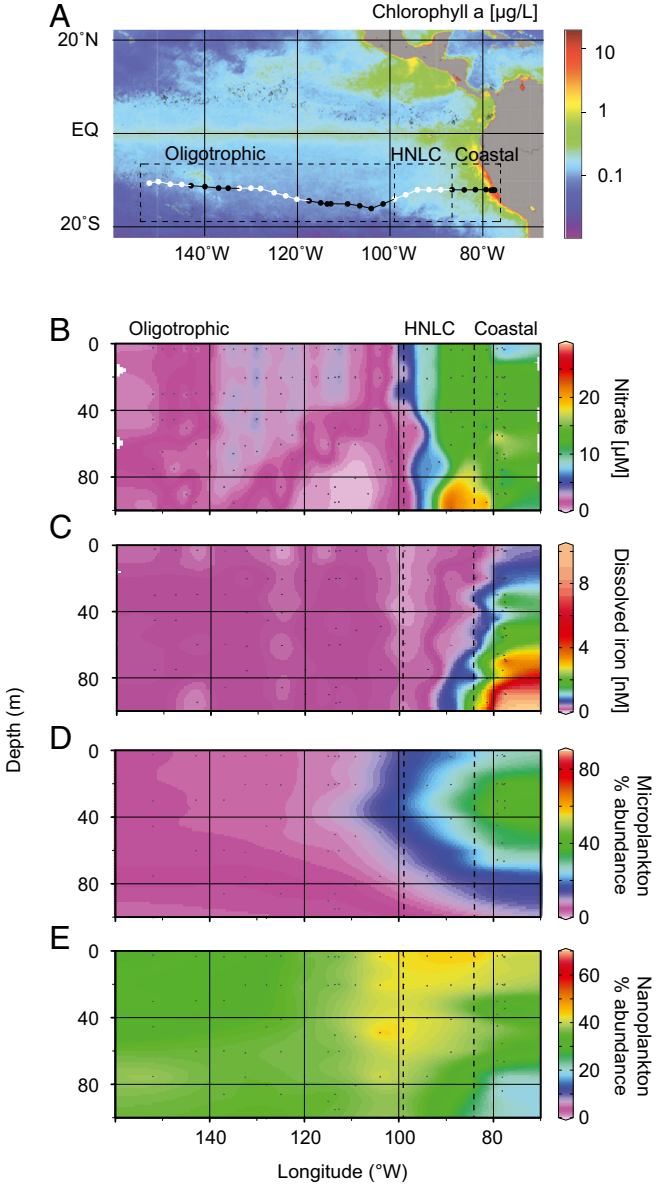

Fig. 1. (*A*) US GEOTRACES EPZT cruise track map with satellite-based average sea surface chlorophyll [Moderate Resolution Imaging Spectroradiometer (MODIS) Aqua, austral summer 2013–2014]. Surface seawater was collected continuously from a trace metal clean tow fish across coastal ([dFe] > 0. 2 nM, sample 1); high-nutrient, low-chlorophyll ([dFe] < 0.2 nM, $[NO_3^-]$ > 5 µM, sample 2); and oligotrophic ($[NO_3^-]$ < 5 µM, samples 3–6) regions. Alternating black and white lines represent the six sampling intervals from which composite samples were collected. (*B* and *C*) Interpolated concentrations of nitrate and dFe. (*D* and *E*) Phytoplankton community composition based on pigment analysis.

Results

To investigate iron-binding ligands in coastal, HNLC, and oligotrophic regimes, we sampled near-surface seawater during the 2013 US GEOTRACES Eastern Pacific Zonal Transect (EPZT) cruise GP16 (Fig. 1*A*). At least 27 unique iron-containing compounds were detected by LC-ICPMS across six composite surface water samples (Table S1 and Fig. S1). Using LC-ESIMS, we identified the compound eluting at 22.9 min as the hydrophilic trihydroxamate siderophore ferrioxamine B (Fig. 2 and Fig. S2). The chromatograms also showed a suite of nonpolar siderophores eluting between 35 and 50 min (Fig. 2). Many of these were identified as amphibactins, amphiphilic siderophores composed of a peptidic head group with a fatty acid side chain of variable structure (Fig. S3). Finally, two major iron-organic compounds with monoisotopic masses of 959.429 and 709.372 were also identified at 47.1 and 50.9 min, respectively (Figs. S4–S6). These masses do not appear in a database of 367 known siderophores (14). Tandem mass spectra (MS^2) of the 959.429 *m/z* ion indicate that this compound is structurally related to amphibactins, containing the same iron-binding head group (*Supporting Information* and Figs. S4–S6). Although dozens of other minor but distinct peaks were detected by LC-ICPMS, we were not able to identify their molecular ions by LC-ESIMS due to their low abundance and ion suppression from coeluting compounds. These compounds could potentially also represent siderophores or similar strong Fe–ligand complexes.

There was a clear trend in the abundance of different siderophores across the three nutrient regimes. Hydrophilic siderophores with retention times between 18 and 28 min were most abundant in the coastal sample. To detect the presence of uncomplexed siderophores, we titrated samples with iron to saturate all strong ligands. In the coastal upwelling sample, no changes in iron-bound siderophore concentration were observed (Fig. 2), indicating that siderophores in this region were fully complexed with iron, consistent with the relatively high ambient dissolved iron concentrations (0.1–1.1 nM, average 0.4 nM; Fig. 1*C*). The elevated baseline observed upon iron addition is indicative of a large excess of chromatographically unresolved organic compounds that can act as weak iron-binding ligands (Fig. 2*A*). These structurally heterogeneous compounds were found at similar concentrations across all samples and are most likely background refractory organic compounds such as humic substances (6).

In the HNLC sample, the siderophore composition changed dramatically. Hydrophilic siderophores were less abundant, whereas amphiphilic siderophores (amphibactins and amphibactin-like siderophores) and overall siderophore concentration were fivefold higher (Fig. 2*C*). This change coincided with a decrease in dFe to 0.03–0.07 nM (average 0.05 nM) and an increase in the abundance of uncomplexed siderophores, which here make up 40% of the total. Across the oligotrophic region, amphiphilic siderophore concentrations declined farther offshore, and hydrophilic siderophores returned. As with the HNLC regime, ambient dFe concentrations were low (0.05–0.12 nM, average

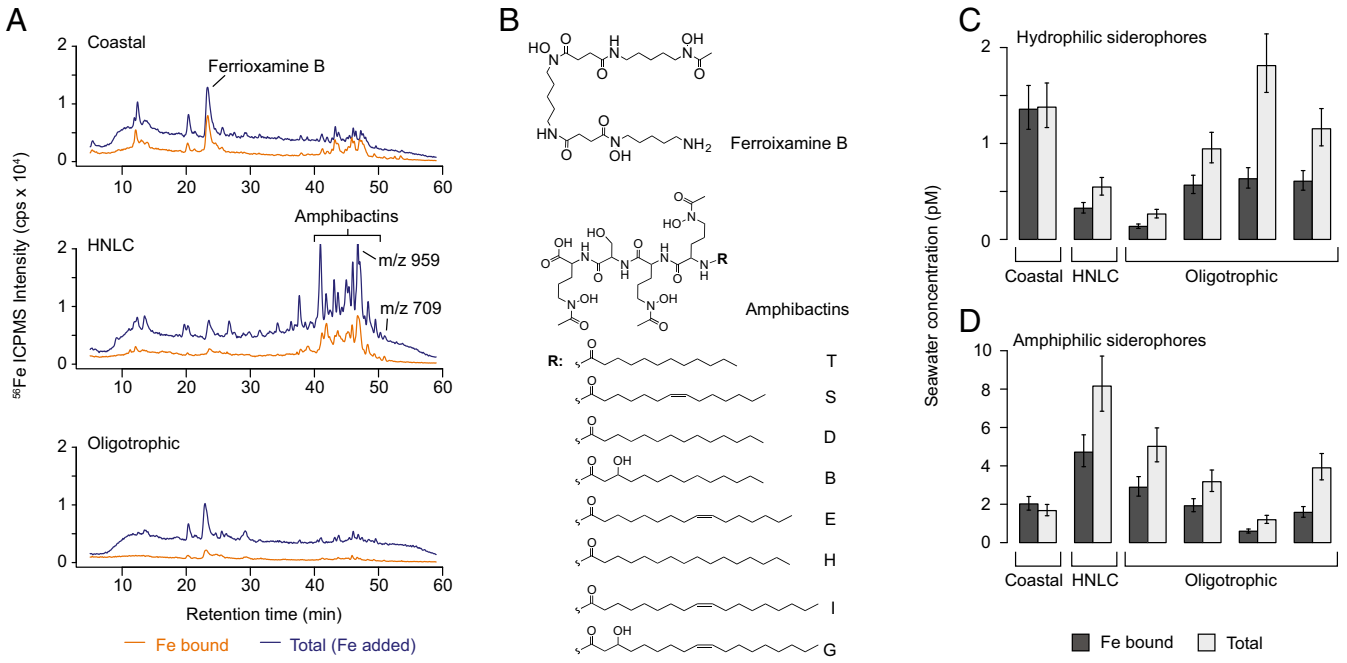

Fig. 2. (*A*) Representative LC-ICPMS chromatograms of samples collected from the coastal, HNLC, and oligotrophic surface ocean. The orange line indicates ligands bound to naturally occurring iron, whereas the blue line indicates total ligand after addition of excess iron to saturate uncomplexed ligands. The major peaks at 23 min and between 40 and 50 min were identified as the siderophores ferrioxamine B and amphibactins B-T. (*B*) Structures of ferrioxamine B and amphibactins B-T. (*C* and *D*) Concentrations of hydrophilic siderophores (eluting between 18 and 28 min) and amphiphilic siderophores (eluting between 35 and 55 min). These total concentrations are anticorrelated ($r^2 = 0.65$). Error bars represent the analytical uncertainty ($\pm 2\sigma$).

0.07 nM), and a large fraction of siderophores (40–65%) were not complexed with iron. Because dFe is higher than total siderophore concentration (3–9 pM) in the HNLC and oligotrophic samples, the presence of a large fraction of iron-free siderophores is notable. One possible explanation is that most dFe is tightly complexed by other strong ligands that can compete with siderophores for iron (6). Alternatively, the ligand exchange kinetics of dFe may be slow relative to the turnover time of iron-free siderophores. Under either scenario, a significant proportion of the total siderophores in these low-iron regions is available to enhance the dissolution of iron from particulate phases or atmospheric dust (15). Iron-bound ferrioxamines and amphibactins only account for a portion of the total dFe (up to 10%), whereas ambient strong ligand concentrations measured by competitive ligand exchange voltammetry methods are generally in excess of dFe (6). This suggests that additional organic ligands that were not captured by the solid phase extraction resin such as polar metabolites, humic substances, and acidic polysaccharides may also be present in these surface waters.

We investigated the potential microbial sources of these siderophores by surveying the prevalence of the biosynthesis genes within known marine bacterial genomes and metagenomes. Ferrioxamine biosynthesis genes (DesA-D) are present in many different microbial taxa including some strains of *Salinispora*, *Micrococcus*, *Arthrobacter*, *Streptomyces*, *Micromonospora*, *Pseudomonas*, *Marinobacter*, and *Erwinia* (16–19). Using these genes as query sequences, a search for DesA-D homologs within the *Tara* Oceans expedition metagenomic catalog (20) yielded many sequences with >50% amino acid identity. However, few of these *Tara* genes closely matched the query sequences (>90% identity), and evaluating whether the more distant homologs have the same functionality remains a challenge. Thus, these ferrioxamine biosynthesis genes were not pursued further.

Although ferrioxamine biosynthesis has been widely investigated across many microbial taxa due to its pharmaceutical importance, amphibactin biosynthesis has only been studied in a few organisms, including several unsequenced *Vibrio* strains and *Alcanivorax borkumensis* SK2 (21). However, amphibactins may play a particularly important role due to their high concentration in the HNLC eastern Pacific. In *Alcanivorax*, an oil-degrading Gammaproteobacterium, the iron-binding head group of amphibactin is assembled by a pair of nonribosomal peptide synthetase (NRPS) enzymes, ABO_2093 and ABO_2092 (21), although the proteins involved in the activation and addition of the fatty acid side chain are still unknown. Peptide order in NRPS genes is controlled by modular adenylation domains; ABO_2093 contains three domains that link together N^5-acyl N^5-hydroxy ornithine, N^5-acyl N^5-hydroxy ornithine, and serine. ABO_2092 has a single domain that attaches the final N^5-acyl N^5-hydroxy ornithine. These domains possess binding pocket sequences that are specific for the incorporated peptide, enabling the product of NRPS genes to be predicted in silico (22) and providing a means to evaluate the function of genes that have lower (<90%) amino acid identity to ABO_2093 and ABO_2092.

To investigate diversity in the phylogeny of amphibactin producing bacteria, we searched for homologs to these two biosynthesis genes in GenBank. We identified similar sequences to ABO_2092 and ABO_2093 that were collocated in the genomes of numerous marine *Vibrio* species, and we verified their likely identity as amphibactin biosynthethic genes via in silico prediction algorithms (22). As further evidence, we cultured five of these strains under iron limited conditions, and confirmed the production of amphibactins by LC-ESIMS (*Supporting Information*).

We next used the presumptive *Alcanivorax* and *Vibrio* NRPS biosynthetic genes to aid in identifying homologous genes within the *Tara* Oceans metagenomic catalog (20). These genes were screened for the presence of adenylation domains that are indicative of amphibactin production. Phylogenetic analyses (Fig. 3*A*) identified homologs from the *Tara* Oceans microbial reference gene catalog (OM-RGC) (20) that were related to the NRPS biosynthetic genes from siderophore-producing bacteria. For ABO_2093, three of these genes (OM-RGC.v.1.000002136, 000002106, and 000002128) predicted all three adenylation domains, whereas others appeared to be incomplete assemblies

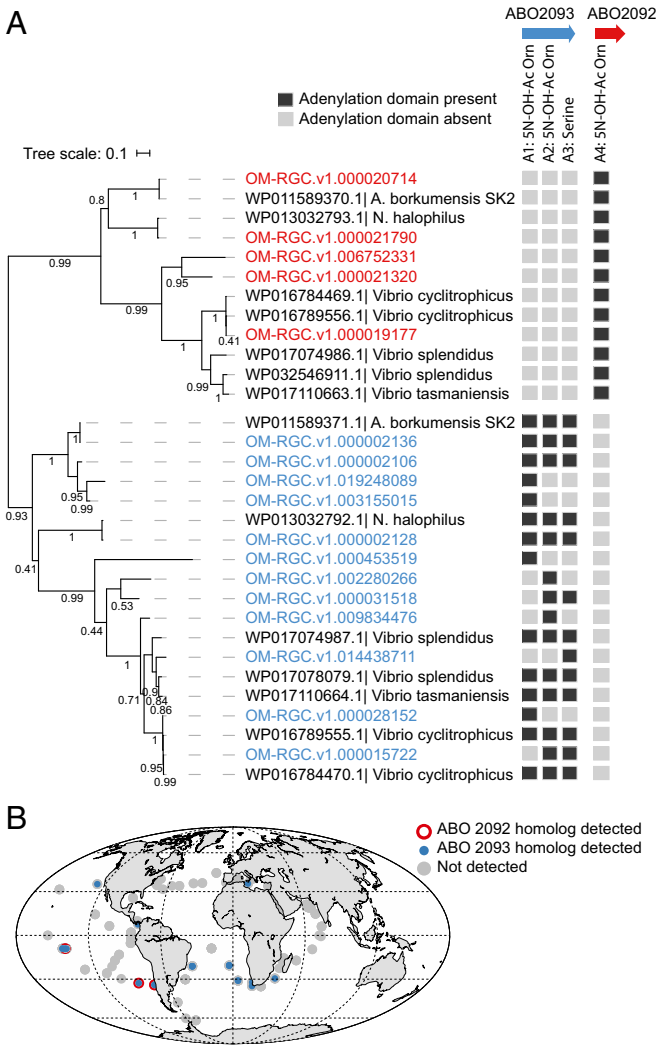

Fig. 3. (*A*) Phylogenetic tree of amphibactin nonribosomal peptide synthetase genes from cultured organisms (GenBank) and from the *Tara* OM-RGC (20). Adenylation domains detected by in silico prediction (22) are shown. Scale bar represents 0.1 substitutions per site. (*B*) Geographic locations of >1× coverage of amphibactin NRPS genes within the OM-RGC.

that possess one or two of the three domains. It is also possible that these incomplete genes may be part of biosynthetic pathways for other N^5-acyl N^5-hydroxy ornithine-containing siderophores that are structurally similar to amphibactin.

The presence of ABO_2092 and ABO_2093 genes across the *Tara* Oceans expedition samples was then investigated. Both amphibactin NRPS biosynthetic genes cooccurred in samples from the eastern tropical South Pacific (Fig. 3*B*), in close proximity to sites where amphibactins were measured in our study. These findings are consistent with predictions that the sequences identified in Fig. 3*A* likely represent at least a subset of the amphibactin biosynthetic genes from bacteria that inhabit the eastern tropical South Pacific. We also detected amphibactin NRPS genes in other regions characterized by low dFe concentrations, such as the equatorial Pacific and South Atlantic Ocean (23). Because conservative criteria were used to detect the presence of amphibactin genes, their absence elsewhere does not necessarily indicate the absence of amphibactin-producing microbes. Other contributing factors may be limitations of the sequencing depth of each metagenome as well as the likely existence of other amphibactin NRPS sequences that are not represented in Fig. 3*A*.

Discussion

It is well established that strong iron ligands are present throughout the ocean, but the chemical identity of these compounds has remained largely unknown. By identifying siderophores as a fraction of the strong ligand pool, we demonstrate that the composition of strong ligands changes significantly across different nutrient regimes. In coastal and oligotrophic regions, the siderophore ferrioxamine B was the most abundant compound detected, which is consistent with previous observations of ferrioxamine B across the iron-replete North Atlantic Ocean (12). Although iron is generally not considered a limiting nutrient in these regions, some microbes may have iron requirements that can only be met by siderophore-mediated acquisition. In the HNLC region characterized by low dFe relative to nitrate concentrations, ferrioxamines decreased in abundance. However, the total concentration of siderophores increased due to the appearance of amphiphilic siderophores. These changes in siderophore composition could potentially affect rates of iron regeneration, dissolution, scavenging, and uptake. Modeling this variability is one of the major hurdles for realistic global biogeochemical simulations of marine iron cycling (24). Because ligand composition and sources are unknown, current models are forced to assume a uniform ligand composition with a generic conditional stability constant throughout the ocean. Our results represent a first step toward modeling multiple ligand pools by revealing key components that are linked to specific nutrient regimes.

The high concentrations of free and iron-complexed amphibactins observed in the HNLC tropical South Pacific suggest that microbial iron acquisition strategies are inherently different across this region and that amphibactin-mediated iron acquisition confers a specific competitive advantage to microbes that inhabit HNLC environments. Peptidic compounds have lifetimes on the order of days in the surface ocean (25, 26), and thus, increased siderophore concentrations in HNLC regions likely reflect a balance between local production and consumption. Because iron is chronically limiting in these regions, a decrease in the biological demand for siderophores is unlikely to account for the relative increase in siderophore concentrations. Instead, higher concentrations of amphibactins in the HNLC regions probably reflect greater relative production of siderophores in response to lower iron concentrations. It is also possible that other siderophores are actively produced and consumed in these areas but may be lower in abundance due to rapid cycling or photochemical degradation or may not be captured by the solid phase extraction.

Competition in dilute, iron-poor environments likely selects for microbes based on the effectiveness of their iron acquisition strategies (27). Under such conditions, amphibactins may provide an advantage over more hydrophilic siderophores because the fatty acid side chain of the molecule can partition into cell membranes (28), which may reduce the metabolic cost of diffusive losses (11). The prevalence of hydrophilic siderophores in other regions of the study area implies that the amphiphilic strategy comes at a cost. Ferrioxamine B has a particularly high conditional stability constant for iron (29). It is possible that ferrioxamines are more effective than amphibactins at competing for iron bound to other dissolved marine ligands such as humic substances. This would mean that a larger fraction of dFe may be accessible for complexation by ferrioxamines, but they suffer greater loss to the environment; a smaller fraction of dFe may be accessible to complexation by amphibactins, albeit with a greater efficiency of microbial recovery in dilute environments.

Determining precisely which microbes produce siderophores in the eastern South Pacific Ocean remains a challenge and is probably not limited to a single taxon. The known producers of ferrioxamines are diverse and include organic carbon-degrading bacterial taxa of Actinobacteria and Gammaproteobacteria (16–19). These include numerous strains from marine environments (e.g., *Salinispora tropica* CNB-440 and *Marinobacter lipolyticus* SM-19) (18, 19). The known producers of amphibactins include marine *Alcanivorax* and *Vibrio*, both members of Gammaproteobacteria (21, 28). Two of the genes within the *Tara* Oceans

catalog also matched NRPS genes from *Nitrosococcus halophilus* (Fig. 3*A*), a marine ammonium-oxidizing Gammaproteobacteria, whose genome encodes the entire gene cluster for amphibactin biosynthesis. Although *Vibrio*, *Alcanivorax*, and *Nitrosococcus* are not particularly dominant taxa in the open ocean, other unsequenced bacteria may also possess the amphibactin biosynthesis gene cluster. There are other amphibactin NRPS homologs within the *Tara* Oceans catalog, such as OM-RGC.v1.000453519, that have no matches within the GenBank database with greater than 60% amino acid identity. This may reflect, in part, an underrepresentation of strains derived from HNLC environments among sequenced microbial isolates. Additional genomic sequences of microbes from the HNLC eastern Pacific Ocean are needed to determine which taxa are capable of producing amphibactins in these waters.

The patchy distribution of amphibactin biosynthesis genes across multiple bacterial orders indicates at least one horizontal transfer of amphibactin biosynthesis genes between bacteria. Only a small subset of all sequenced strains of Vibrionales, Chromatiales, and Oceanospirillales possess the amphibactin gene cluster. Furthermore, the phylogeny of the amphibactin biosynthesis genes does not follow the phylogeny of the strains in which they are found. *Alcanivorax* species are more closely related to *Vibrio* than to *Nitrosococcus* species (30), yet the amphibactin NRPS biosynthetic genes of *Alcanivorax borkumensis* and *Nitrosococcus halophilus* are more similar to one another (Fig. 3*A*), suggesting a gene transfer event. Acquisition of amphibactin biosynthetic gene clusters by horizontal gene transfer may be one mechanism by which certain microbes can adapt to iron-poor HNLC regions. Similar mechanisms have been proposed to explain how certain clades of *Prochlorococcus* adapt to tropical HNLC surface waters. Single-cell genomic studies have reported that *Prochlorococcus* ecotypes that thrive in low-iron, high-phosphate regions appear to have horizontally acquired genes for using organically bound iron (31). Such adaptive strategies may also complement other mechanisms, such as reducing iron quotas via loss of genes encoding iron-containing proteins (32).

The role of siderophores in the surface ocean is likely linked to recycling bioavailable iron. Efficient recycling of iron from the biotic pool accounts for up to 90% of dFe uptake in iron-deficient regions of the ocean (33). In the process of microbial mortality induced by grazing and viral lysis, cellular iron is released to the dissolved phase bound to proteins, heme, and other metabolites. Bacteria that consume these compounds may produce siderophores as a means of capturing regenerated iron before it is scavenged by sinking particles. Indeed, the production of ferrioxamines and amphibactins by mixed marine bacterial communities is stimulated by amendments of glucose, glycerol, and chitin (12, 34). Siderophores may also provide a source of bioavailable iron for phytoplankton. Many marine phytoplankton, including diatoms, haptophytes, and cyanobacteria, exhibit similar capacities for taking up iron bound to siderophores, potentially via an enzymatic or indirect (e.g., photochemical) reductive mechanism (13). Furthermore, some phytoplankton and bacterioplankton may express siderophore uptake transporters, even if they cannot produce the compounds themselves (31). Thus, although little is known about the dominant mechanisms for iron acquisition in HNLC regions, it seems likely that amphibactins (which account for 10% of the total dFe) may be an important source of iron for many members of the microbial community. Assuming a cellular iron to phosphorus (Fe:P) quota of 2–8 mmol/mol (35) and Redfield cellular N:P (16:1), we estimate that microbes require ~5–25 pM Fe per day to sustain the N uptake rate of ~50 nM/d characteristic of the eastern tropical South Pacific HNLC region (36). At 9 pM total siderophore concentrations, daily cycling could transfer regenerated iron into siderophores and sustain a significant fraction of the microbial community.

Conclusion

The changes in siderophore composition and concentrations across different nutrient regimes of the eastern tropical Pacific Ocean provide evidence that siderophores are an active component of microbial iron cycling. The highest concentrations of free and iron-complexed siderophores were found in the iron-poor HNLC region, where amphibactins represented >90% of the siderophores that we were able to quantify. Altogether, this suggests that the distinct distribution of these compounds reflects microbial adaptations for survival in specific nutrient regimes. Furthermore, evidence for horizontal transfer of the amphibactin gene cluster across diverse Gammaproteobacteria suggests a possible mechanism by which some microbes may have acquired siderophore production and uptake abilities that could provide them with a competitive advantage in iron-poor niches of the ocean. Because these amphiphilic siderophores can be tethered to cell membranes (28), new questions arise as to the energetic trade-offs that select for specific siderophores, the partitioning of siderophores between dissolved and particulate phases, and the availability of various siderophores to the microbial community at large. Furthermore, many different amphiphilic siderophores have been identified in marine microbes (37), and further surveys of other iron-starved regions may reveal a broader suite of siderophores produced under different environmental conditions. The composition and concentration of siderophores potentially affect rates of iron regeneration, dissolution, scavenging, and uptake. Unraveling the cycling of siderophores is therefore an important element to understanding patterns of microbial productivity across the ocean.

Methods

Sample Collection and Processing. The sample collection method used in this study was designed to minimize metal contamination and sample processing (e.g., pH changes) to preserve the iron-organic compounds intact. Trace metal clean filtered seawater was pumped by a tow-fish from 3 m depth along the cruise track of the US GEOTRACES EPZT (GP16) cruise from October to December 2013 (Table S2). Thus, each sample represents an integrated average signal across a wide region. Between 400 and 600 L of seawater was filtered continuously at a flow rate of 250 mL/min and extracted through custom-made solid phase extraction (SPE) columns packed with 20 g resin (Bondesil ENV; Agilent). Before sample collection, SPE columns were primed with distilled methanol, flushed with ultrahigh-purity water (qH_2O), acidified to pH 2 with dilute HCl, and finally rinsed with qH_2O. Although the methods used to extract and separate iron-binding compounds from seawater in this study are capable of extracting and detecting a wide variety of ligands including many types of hydroxamate and alpha hydroxy carboxylic acid-based siderophores, there are likely additional ligands of potential importance in seawater that are not captured or strongly retained by these solid phases. Adjustments to the extraction methods and chromatography of the LC-ICPMS-ESIMS approach described here may continue to uncover different strategies for iron acquisition across the ocean. Samples were stored at −20 °C and returned to the laboratory for further analyses. Thawed SPE columns were rinsed with 500 mL of qH_2O, to remove salts, and organic ligands were eluted with 250 mL of methanol (MeOH). Extracts were concentrated by rotary evaporation, and the final volume was adjusted to 6 mL with qH_2O. Samples were stored at −20 °C in polytetrafluoroethylene (PTFE) vials. Aliquots (1 mL) of each concentrated sample were removed and spiked with 20 μL of 50 μM cyanocobalamin as an internal standard. A sample blank was also collected by pumping 200 mL of filtered seawater through an SPE column, which was frozen, processed, and analyzed with the six seawater samples. Nitrate and pigment samples were collected and analyzed as described previously (38, 39).

Liquid Chromatography. Organic extracts were separated on an Agilent 1260 series bioinert high-pressure liquid chromatography (HPLC) system fitted with a C8 column (2.1 × 100 mm, 3-μm particle size; Hamilton) and polyetheretherketone (PEEK) tubing and connectors. Ligands were eluted with solvent A (5 mM aqueous ammonium formate) and solvent B (5 mM ammonium formate in distilled MeOH) using a 50-min gradient from 10 to 90% B, followed by isocratic elution at 90% B for 10 min at a flow rate of 0.2 mL/min. A postcolumn PEEK flow splitter directed 50 μL/min into the ICPMS or ESIMS.

Inductively Coupled Plasma Mass Spectrometry. The method for LC-ICPMS analysis was modified from Boiteau et al. (40). The flow of the LC column was coupled directly to a quadrupole ICPMS (iCAP Q; Thermo Scientific) using a

perfluoroalkoxy micronebulizer (PFA-ST; Elemental Scientific) and a cyclonic spray chamber cooled to 0 °C. Oxygen gas was introduced to the plasma at 25 mL/min to prevent the deposition of reduced organics on the cones. The ICPMS was equipped with platinum sampler and skimmer cones. ^{56}Fe, ^{57}Fe, and ^{59}Co were monitored with an integration time of 0.05 s each. Measurements were made in kinetic energy discrimination mode with a He collision gas introduced at a rate of 4.2 mL/min to remove ArO^+ interferences on ^{56}Fe. Peak areas were integrated and used to calculate concentrations with a six-point calibration curve of a ferrioxamine E standard solution (retention time = 19.8 min). Because only the iron-bound form is quantified by LC-ICPMS, samples were titrated with excess iron citrate and reanalyzed to quantify total siderophore concentrations. A 1:10 addition of the iron citrate stock solution was sufficient to saturate the unbound iron complexes.

Electrospray Ionization Mass Spectrometry Analysis. For determination of the siderophore mass, the flow from the LC was coupled to an Orbitrap Fusion mass spectrometer (Thermo Scientific) equipped with a heated electrospray ionization source. Electrospray ionization source parameters were set to a capillary voltage of 3500 V; sheath, auxiliary, and sweep gas flow rates of 12, 6, and 2 (arbitrary units); and ion transfer tube and vaporizer temperatures of 300 and 75 °C. Mass spectra scans were collected in high-resolution (450 K) positive mode. High-energy collision-induced dissociation (HCD) MS^2 spectra were collected on the ion trap mass analyzer. Ions were trapped using a quadrupole isolation window of 1 *m/z* and were then fragmented using an HCD collision energy of 35%. Details of data analysis (41) are provided in *Supporting Information*.

ACKNOWLEDGMENTS. We thank B. Twining and B. Bidigare for pigment community data; NASA Ocean Biology Processing Group for Moderate Resolution Imaging Spectroradiometer (MODIS) Aqua chlorophyll data (oceancolor.gsfc.nasa.gov); and C. McLean, P. Arevalo, M. Cutler, and M. Polz for assistance with selecting and growing *Vibrio* strains. We are grateful to chief scientists J. Moffett and C. German; G. Smith for sampling assistance; R. Bundy, L. Ouerdane, and O. Donard for valuable discussion; B. Sohst and the Oceanographic Data Facility for iron and nitrate data; and the scientists and crew of the R/V *Thomas G. Thompson*. Support was provided by the National Science Foundation (NSF) program in chemical oceanography (OCE-1356747, OCE-1233261, and OCE-1237034), the NSF Science and Technology Center for Microbial Oceanography Research and Education (DBI-0424599), the European Molecular Biology Organization (Long Term Fellowship ALTF 721-2015), the European Commission (LTFCOFUND2013, GA-2013-609409), the Gordon and Betty Moore Foundation (Grants GBMF3298 and GBMF3934), and the Simons Foundation Simons Collaborative on Ocean Processes and Ecology (329108).

1. Morel FMM, Price NM (2003) The biogeochemical cycles of trace metals in the oceans. *Science* 300(5621):944–947.
2. Boyd PW, Ellwood MJ (2010) The biogeochemical cycle of iron in the ocean. *Nat Geosci* 3(10):675–682.
3. Resing JA, et al. (2015) Basin-scale transport of hydrothermal dissolved metals across the South Pacific Ocean. *Nature* 523(7559):200–203.
4. Hutchins DA, et al. (2002) Phytoplankton iron limitation in the Humboldt Current and Peru Upwelling. *Limnol Oceanogr* 47(4):997–1011.
5. Bruland KW, Rue EL, Smith GJ, DiTullio GR (2005) Iron, macronutrients and diatom blooms in the Peru upwelling regime: Brown and blue waters of Peru. *Mar Chem* 93(2-4):81–103.
6. Gledhill M, Buck KN (2012) The organic complexation of iron in the marine environment: A review. *Front Microbiol* 3:69.
7. Wells ML, Trick CG (2004) Controlling iron availability to phytoplankton in iron-replete coastal waters. *Mar Chem* 86(1-2):1–13.
8. Hassler CS, Schoemann V, Nichols CM, Butler ECV, Boyd PW (2011) Saccharides enhance iron bioavailability to Southern Ocean phytoplankton. *Proc Natl Acad Sci USA* 108(3):1076–1081.
9. Hopkinson BM, Barbeau KA (2012) Iron transporters in marine prokaryotic genomes and metagenomes. *Environ Microbiol* 14(1):114–128.
10. Toulza E, Tagliabue A, Blain S, Piganeau G (2012) Analysis of the global ocean sampling (GOS) project for trends in iron uptake by surface ocean microbes. *PLoS One* 7(2):e30931.
11. Völker C, Wolf-Gladrow DA (1999) Physical limits on iron uptake mediated by siderophores or surface reductases. *Mar Chem* 65(3-4):227–244.
12. Mawji E, et al. (2008) Hydroxamate siderophores: Occurrence and importance in the Atlantic Ocean. *Environ Sci Technol* 42(23):8675–8680.
13. Lis H, Shaked Y, Kranzler C, Keren N, Morel FMM (2015) Iron bioavailability to phytoplankton: An empirical approach. *ISME J* 9(4):1003–1013.
14. Baars O, Morel FMM, Perlman DH (2014) ChelomEx: Isotope-assisted discovery of metal chelates in complex media using high-resolution LC-MS. *Anal Chem* 86(22):11298–11305.
15. Akafia MM, Harrington JM, Bargar JR, Duckworth OW (2014) Metal oxyhydroxide dissolution as promoted by structurally diverse siderophores and oxalate. *Geochim Cosmochim Acta* 141:258–269.
16. Müller G, Raymond KN (1984) Specificity and mechanism of ferrioxamine-mediated iron transport in Streptomyces pilosus. *J Bacteriol* 160(1):304–312.
17. Smits THM, Duffy B (2011) Genomics of iron acquisition in the plant pathogen Erwinia amylovora: Insights in the biosynthetic pathway of the siderophore desferrioxamine E. *Arch Microbiol* 193(10):693–699.
18. Amin SA, Green DH, Al Waheeb D, Gärdes A, Carrano CJ (2012) Iron transport in the genus Marinobacter. *Biometals* 25(1):135–147.
19. Roberts AA, Schultz AW, Kersten RD, Dorrestein PC, Moore BS (2012) Iron acquisition in the marine actinomycete genus Salinispora is controlled by the desferrioxamine family of siderophores. *FEMS Microbiol Lett* 335(2):95–103.
20. Sunagawa S, et al.; Tara Oceans coordinators (2015) Ocean plankton. Structure and function of the global ocean microbiome. *Science* 348(6237):1261359.
21. Kem MP, Zane HK, Springer SD, Gauglitz JM, Butler A (2014) Amphiphilic siderophore production by oil-associating microbes. *Metallomics* 6(6):1150–1155.
22. Bachmann BO, Ravel J (2009) Chapter 8. Methods for in silico prediction of microbial polyketide and nonribosomal peptide biosynthetic pathways from DNA sequence data. *Methods Enzymol* 458(9):181–217.
23. Moore CM, et al. (2013) Processes and patterns of oceanic nutrient limitation. *Nat Geosci* 6(9):701–710.
24. Tagliabue A, et al. (2016) How well do global ocean biogeochemistry models simulate dissolved iron distributions? *Global Biogeochem Cycles* 30(2):149–174.
25. Keil RG, Kirchman DL (1999) Utilization of dissolved protein and amino acids in the northern Sargasso Sea. *Aquat Microb Ecol* 18(3):293–300.
26. Wei L, Ahner BA (2005) Sources and sinks of dissolved phytochelatin in natural seawater. *Limnol Oceanogr* 50(1):13–22.
27. Maldonado MT, et al. (2001) Iron uptake and physiological response of phytoplankton during a mesoscale Southern Ocean iron enrichment. *Limnol Oceanogr* 46(7):1802–1808.
28. Martinez JS, et al. (2003) Structure and membrane affinity of a suite of amphiphilic siderophores produced by a marine bacterium. *Proc Natl Acad Sci USA* 100(7):3754–3759.
29. Hider RC, Kong X (2010) Chemistry and biology of siderophores. *Nat Prod Rep* 27(5):637–657.
30. Williams KP, et al. (2010) Phylogeny of gammaproteobacteria. *J Bacteriol* 192(9):2305–2314.
31. Malmstrom RR, et al. (2013) Ecology of uncultured Prochlorococcus clades revealed through single-cell genomics and biogeographic analysis. *ISME J* 7(1):184–198.
32. Rusch DB, Martiny AC, Dupont CL, Halpern AL, Venter JC (2010) Characterization of Prochlorococcus clades from iron-depleted oceanic regions. *Proc Natl Acad Sci USA* 107(37):16184–16189.
33. Boyd PW, et al. (2015) Why are biotic iron pools uniform across high- and low-iron pelagic ecosystems? *Global Biogeochem Cycles* 29(7):1028–1043.
34. Mawji E, et al. (2011) Production of siderophore type chelates in Atlantic Ocean waters enriched with different carbon and nitrogen sources. *Mar Chem* 124(1-4):90–99.
35. Twining BS, et al. (2011) Metal quotas of plankton in the equatorial Pacific Ocean. *Deep Res Part II Top Stud Oceanogr* 58(3-4):325–341.
36. Dugdale RC, Wilkerson FP (1991) Low specific nitrate uptake rate: A common feature of marine ecosystems. *Limnol Oceanogr* 36(8):1678–1688.
37. Sandy M, Butler A (2009) Microbial iron acquisition: Marine and terrestrial siderophores. *Chem Rev* 109(10):4580–4595.
38. Hydes D, et al. (2010) Determination of dissolved nutrients (N, P, Si) in seawater with high precision and inter-comparability using gas-segmented continuous flow analysers. *The GO-SHIP Repeat Hydrography Manual: A Collection of Expert Reports and Guidelines* (United Nations Educational, Scientific and Cultural Organization, Paris), IOCCP Report 14, ICPO Publication Series 134, pp 1–87.
39. Hooker SB, et al. (2005) The second SeaWiFS HPLC analysis round-robin experiment (SeaHARRE-2). *NASA Tech Memo 2005-212785* (NASA Goddard Space Flight Center, Greenbelt, MD).
40. Boiteau RM, Fitzsimmons JN, Repeta DJ, Boyle EA (2013) Detection of iron ligands in seawater and marine cyanobacteria cultures by high-performance liquid chromatography-inductively coupled plasma-mass spectrometry. *Anal Chem* 85(9):4357–4362.
41. Boiteau RM, Repeta DJ (2015) An extended siderophore suite from Synechococcus sp. PCC 7002 revealed by LC-ICPMS-ESIMS. *Metallomics* 7(5):877–884.
42. Sedwick PN, Sohst BM, Ussher SJ, Bowie AR (2015) A zonal picture of the water column distribution of dissolved iron(II) during the U.S. GEOTRACES North Atlantic transect cruise (GEOTRACES GA03). *Deep Res Part II Top Stud Oceanogr* 116:166–175.
43. Vraspir JM, Holt PD, Butler A (2011) Identification of new members within suites of amphiphilic marine siderophores. *Biometals* 24(1):85–92.
44. Eddy SR (2011) Accelerated profile HMM searches. *PLOS Comput Biol* 7(10):e1002195.
45. Huerta-Cepas J, Dopazo J, Gabaldón T (2010) ETE: A Python environment for tree exploration. *BMC Bioinformatics* 11(1):24.
46. Sievers F, et al. (2011) Fast, scalable generation of high-quality protein multiple sequence alignments using Clustal Omega. *Mol Syst Biol* 7(1):539.
47. Wallace IM, O'Sullivan O, Higgins DG, Notredame C (2006) M-Coffee: Combining multiple sequence alignment methods with T-Coffee. *Nucleic Acids Res* 34(6):1692–1699.
48. Capella-Gutiérrez S, Silla-Martínez JM, Gabaldón T (2009) trimAl: A tool for automated alignment trimming in large-scale phylogenetic analyses. *Bioinformatics* 25(15):1972–1973.
49. Guindon S, et al. (2010) New algorithms and methods to estimate maximum-likelihood phylogenies: Assessing the performance of PhyML 3.0. *Syst Biol* 59(3):307–321.
50. Stamatakis A (2014) RAxML version 8: A tool for phylogenetic analysis and post-analysis of large phylogenies. *Bioinformatics* 30(9):1312–1313.